Published in final edited form as:
FEMS Immunol Med Microbiol. 2008 June ; 53(1): 72–78. doi:10.1111/j.1574-695X.2008.00395.x.

Respiratory infection with *Francisella novicida* induces rapid dystrophic cardiac calcinosis (DCC)

Kimberly M. Roth[1], **Steve Oghumu**[1], **Anjali A. Satoskar**[2], **John S. Gunn**[3], **Nico van Rooijen**[4], and **Abhay R. Satoskar**[1]

[1]Department of Microbiology, The Ohio State University, Columbus, OH, USA [2]Department of Pathology, The Ohio State University, Columbus, OH, USA [3]Center for Microbial Interface Biology, The Ohio State University, Columbus, OH, USA [4]Department of Cell Biology and Immunology, Free University, Amsterdam, The Netherlands

Abstract

Francisella tularensis causes pulmonary tularemia and death in humans when left untreated. Here, using a novel aerosol infection model, we show that acute pulmonary *Francisella novicida* infection not only causes pneumonia and liver damage, but also induces dystrophic cardiac calcinosis (DCC) in BALB/c mice. C57BL/6 mice also develop pneumonia and hepatic damage, but fail to develop DCC. Development of DCC in BALB/c mice is associated with significant induction of RANKL but not osteopontin in their organs. Depletion of lung macrophages prior to infection markedly reduces pericarditis and calcification in BALB/c mice but does not increase their susceptibility to infection.

Keywords

Francisella novicida; pericardial calcification; osteopontin; aerosol infection

Introduction

Although the natural incidence of pulmonary tularemia is extremely low, the high infectivity, rapid dissemination and the severity of the disease caused by *Francisella tularensis* dictates its classification as a Group A bioterror agent (Dennis *et al.*, 2001). Aerosol exposure of mice to *Francisella novicida*, a subspecies of *F. tularensis*, which is nonpathogenic for humans, results in fatal pneumonia and liver pathology that mimics respiratory tularemia in humans.

Francisella tularensis DNA has been detected previously in the cardiac tissue of infected patients and endocarditis has been observed in rhesus monkeys (Hall *et al.*, 1973; Lamps *et al.*, 2004), but there are no reports of pericardial calcification following aerosol infection with *Francisella*. Dystrophic cardiac calcinosis (DCC) results from injury to the heart in certain inbred strains of mice such as BALB/c and DBA/2, and is characterized by the formation of calcified plaques on the pericardium (O'Regan & Berman, 2000). Several studies have linked calcification in mice with the *Dyscalc* genetic loci as well as osteopontin and RANKL, two cytokines which play an integral role in both cellular immune responses

Correspondence: Abhay R. Satoskar, Department of Microbiology, The Ohio State University, 484 West 12th Avenue, OH 43210, Columbus, USA. Tel.: +1 614 292 3243; fax: +1 614 247 8240; satoskar.2@osu.edu.

and inflammation (O'Regan & Berman, 2000; Aherrahrou *et al.*, 2004; Collin-Osdoby, 2004). While some reports suggest that osteopontin is involved in inducing DCC (Aherrahrou *et al.*, 2004), others indicate that osteopontin is required for its prevention (Giachelli *et al.*, 2005). RANKL is produced during inflammation and is a natural ligand for RANK, which is expressed on the surface of macrophages and dendritic cells. Unlike osteopontin, it is widely accepted that RANKL promotes calcification via its interaction with RANK. DCC has many causes, including hormonal treatments, and chronic viral and bacterial infections, however, it has never been reported in acute infection (O'Regan & Berman, 2000).

In this study, we found that unlike C57BL/6 mice, BALB/c mice produce high levels of RANKL, but fail to up-regulate osteopontin production in their heart and lung tissue during acute pulmonary infection with *F. novicida* and develop DCC. We also show that pulmonary macrophages are involved in the pathogenesis of DCC during *F. novicida* infection.

Materials and methods

Eight- to 10-week-old, pathogen-free, sex-matched BALB/c and C57BL/6 mice were purchased from Harlan (Indianapolis, IN). Both strains were anesthetized and infected by delivering 10^3 *F. novicida* CFU in 50 μL directly into the trachea using a MicroSprayer™ aerosolizer, model A1C (Penn-Century Inc., Philadelphia, PA) (Beck *et al.*, 2002). Animals were housed and maintained under institutional guidelines for animal research at The Ohio State University. For survival studies, animals were monitored every 8 h for survival following aerosol infection and time of death was recorded. In other experiments, three- to four mice from each group were euthanized every 24 h after aerosol challenge and the lung, liver and heart were harvested for histopathology and quantifying mRNA levels of osteopontin and RANKL by real-time PCR. Sera were collected to measure levels of tumor necrosis factor (TNF)-α, IFN-γ and IL-12p70 (BD-PharMingen) by enzyme-linked immunosorbent assay (ELISA). For histological analysis, hematoxylin&eosin (H&E) staining was performed on all tissue samples, while von Kossa staining was performed on the heart tissue to evaluate calcium deposition. The course of pathology in the organs of both strains was monitored daily. H&E stained sections of the lungs, livers and hearts from infected BALB/c and C57BL/6 mice were blinded, analyzed and scored for severity of inflammation by a pathologist. For lungs, Grade I inflammation was mild and characterized by an occasional alveoli filled with scattered few macrophages, neutrophils and lymphocytes. Grade II inflammation was moderate and characterized by foci of inflammatory cells around the bronchi and many alveolar spaces filled with inflammatory cells. Grade III inflammation was pneumonia of the whole lung characterized by almost all alveoli filled with inflammatory exudate comprised of neutrophils, macrophages and necrotic cell debris, and microabscesses. For liver, Grade I inflammation was mild and characterized by focal infiltrate of macrophages and lymphocytes. Grade II inflammation was moderate characterized by at least two foci of inflammation per high power field. Grade II inflammation was severe and was characterized by tissue damage and more than three foci of inflammation per high power field. For heart, Garde I pericarditis was mild and characterized by focal infiltrate of scattered leukocytes with no calcification. Grade II pericarditis was moderate and characterized by more extensive inflammation and occasional area of pericardial calcification. Grade III pericarditis was characterized by extensive pericardial calcification associated with areas of inflammation. In experiments where lung macrophages were depleted, 100 μL of either clodronate-containing liposomes or phosphate-buffered saline (PBS)-containing liposomes were administered by aerosol, as described above, and mice were rested for 2 days before infection with 10^3 *F. novicida*. Macrophage depletion in the lungs was monitored using flow cytometry and was 95% effective. For real-time reverse transcriptase (RT)-PCR, total RNA was extracted from lung,

liver and heart sections using the Spin or Vacuum (SV) Total RNA Isolation System (Promega), mRNA was reverse transcribed, and cDNA was amplified in an Opticon2 DNA Engine (BioRad) using SYBR Green Taq polymerase. The osteopontin and β-actin primers used to amplify the cDNA in this semi-quantitative RT-PCR were previously described (Zhu *et al.*, 2005). A Kaplan–Meier curve was constructed and a Log-Rank test was applied to determine the statistical significance of survival differences between the two strains of mice or mice that had received different treatments. Student's *t*-test was used for determining the statistical significance of differences in mRNA and cytokine levels. A value of $P < 0.05$ was considered significant.

Results and discussion

Both BALB/c and C57BL/6 mice developed pneumonic tularemia following administration of a single aerosolized dose of *F. novicida* directly into the lower trachea. BALB/c mice succumbed significantly faster to infection compared with C57BL/6 mice when infected with 10^3 CFU of aerosolized *F. novicida* (Fig. 1a), and they were also significantly more susceptible to infection with LVS and as few as 15 CFU of aerosolized *F. novicida* infection than C57BL/6 mice (data not shown). These observations support a recent study by Shen *et al.* (2003) which showed that both BALB/c and C57BL/6 mice are susceptible to aerosol challenge with as few as 10 CFU of virulent *F. tularensis*. However, in contrast to Shen *et al.*, we observed that C57BL/6 mice were less susceptible to infection by aerosolized *F. novicida* and succumbed to infection significantly slower than BALB/c mice. This discrepancy could be due to differences in experimental methods used for delivering aerosolized bacteria, or due to inherent differences in the virulence between the *Francisella* species used. Nonetheless, our findings show that although *F. novicida*-infected C57BL/6 mice survive longer than BALB/c mice, genetic differences alone are not sufficient to prevent the mortality associated with pulmonary tularemia.

To analyze the pathological organ damage induced by *F. novicida* in BALB/c and C57BL/6 mice at the time of death, we compared the histopathology of H&E stained sections from the lungs, livers and hearts temporally. Lungs from BALB/c mice displayed typical pneumonia characterized by an extensive fibrinoinflammatory exudate filling the alveolar spaces, areas of necrosis, and microabscesses (Fig. 1b). In contrast, C57BL/6 mice displayed moderate congestion of the lungs with foci of inflammatory cells around the bronchi (Fig. 1e). Moreover, temporal comparison of H&E stained slides of the lungs demonstrated that BALB/c mice showed more rapid and severe progression of pathology than C57BL/6 mice (Fig. 2a). Livers from both the strains were fragile and those from BALB/c mice showed subcapsular foci of necrosis on gross examination. Microscopy revealed large foci of acute inflammation comprised of macrophages and neutrophils in the periportal and lobular regions in the liver of BALB/c mice (Fig. 1c). Similarly, C57BL/6 mice developed severe liver inflammation but with fewer and smaller foci of acute inflammation (Fig. 1f). In fact, when liver pathology was compared temporally in BALB/c and C57BL/6 mice, no significant difference was found (Fig. 2b). Gross examination of the pericardium of BALB/c, but not C57BL/6, mice revealed extensive calcification, which was confirmed by microscopy using H&E as well as Von Kossa staining (Fig. 1d and h). Similar pericardial calcification was noted following infection with either *F. novicida* or live vaccine strain (LVS). Infected hearts from BALB/c mice showed foci of pericardial inflammation (data not shown). However, no pericarditis or calcification was evident in the hearts of C57BL/6 mice (Fig. 1g and i). Despite the difference in pericardial calcification between both strains of mice, severity of pericarditis was not significantly different between BALB/c and C57BL/6 mice (Fig. 2c). Although little is known about the effect of *F. tularensis* on the heart, *F. tularensis* DNA has been detected in the hearts of patients that died of tularemia (Lamps *et al.*, 2004). Furthermore, another study in the mouse has shown that *F. tularensis* infection

impairs oxidative and metabolic function of the myocardium, resulting in degradation of the myocardial cellular constituents (Ilback *et al.*, 1984). In this study, we were also able to isolate and cultivate bacteria from the pericardium and foci of calcification, which were identified as *F. novicida* by PCR (data not shown). To confirm these findings and ensure that the *F. novicida* DNA present in the heart was not the result of contamination from the blood, we infected BALB/c mice with *F. novicida* expressing green fluorescent protein (GFP) and used fluorescent microscopy to show dissemination of the bacterium into the heart (Fig. 1j) as well as liver (data not shown). Together, these findings indicate that the greater susceptibility of BALB/c mice to *F. novicida* aerosol infection may be due to increased lung pathology early in infection and that *F. novicida* rapidly disseminates to the pericardium following aerosol challenge and may cause heart damage by inducing DCC in BALB/c mice.

Dystrophic cardiac calcinosis occurs in certain predisposed mouse strains such as BALB/c, DBA/2 and C3H/HeJ mice, but not C57BL/6 mice, following damage to the heart (O'Regan & Berman, 2000; Ivandic *et al.*, 2001). Ivandic *et al.* (1996) have proposed that differences between susceptible C3H/HeJ and resistant C57BL/6 strains at the *Dyscalc1* loci on mouse chromosome 7 as the major predisposing factor for DCC. *Dyscalc1* has since been found to encode a trans-activator of transcription for osteopontin and transforming growth factor-β1 (O'Regan & Berman, 2000; Ivandic *et al.*, 2001), which is more induced in strains that are susceptible to DCC. Therefore, we used real-time RT-PCR to compare osteopontin mRNA levels in infected hearts and lungs from BALB/c and C57BL/6 mice. In addition, we also compared mRNA levels of RANKL, which is known to promote calcification. DCC-resistant C57BL/6 mice showed substantial induction of osteopontin mRNA in both their lungs at all time points and hearts at day 1 (Fig. 3a and b) and also showed slightly increased levels of RANKL mRNA in their lungs at day 1 (Fig. 3c). In contrast, BALB/c mice failed to show a significant increase in levels of osteopontin mRNA in their organs (Fig. 3a and b). However, BALB/c mice contained high amounts of RANKL mRNA in their lungs throughout the course of infection, and RANKL mRNA levels surged in their hearts on day 3 postinfection (Fig. 3c and d). These findings suggest that development of DCC in BALB/c mice may be due to their failure to produce optimal amounts of osteopontin, which is required to inhibit RANKL-induced calcification.

Proinflammatory cytokines such as IL-1, IL-6, IL-12, IFN-γ and TNF-α produced during bacterial infections are critical for host defense, but they also mediate immunopathology and cause death if produced in excess. Therefore, we compared serum levels of IL-12, IFN-γ, and TNF-α as well as organ mRNA levels of IL-1, IL-6 and TNF-α in *F. novicida*-infected BALB/c and C57BL/6 mice. No cytokines were detectable in preinfection samples from both strains (data not shown). IL-12 and IFN-γ were detectable in serum samples from both strains on days 1 and 2 post infection, but no statistically significant differences were noted between the groups. On day 3 postinfection, BALB/c mice produced significantly more IL-12 and IFN-γ when compared with C57BL/6 mice (Fig. 3e and f). However, IL-12 and IFN-γ production declined in BALB/c mice on day 4 and both strains contained comparable amounts of IL-12 and IFN-γ in their plasma at this time. BALB/c mice also consistently produced more serum TNF-α than C57BL/6 mice throughout the course of *F. novicida* infection but these differences were statistically not significant (Fig. 3g). No significant differences were noted in the serum levels of IL-6 and IL-10 between the two strains (data not shown). These results suggest that increased mortality in BALB/c mice following aerosol *F. novicida* infection is not due to overproduction of proinflammatory cytokines in the serum.

Because no significant differences in serum cytokine production between BALB/c and C57BL/6 mice following *F. novicida* aerosol challenge, we compared proinflammatory

cytokine production in the infected organs from these mice temporally. We examined induction of IL-1, IL-6 and TNF-α mRNA levels in the lungs, livers and hearts of both mouse strains. On day 1 postinfection, C57BL/6 mice produced significantly more IL-1 and IL-6, but not TNF-α, in their lungs than the BALB/c mice (Fig. 4a, d and g). However, production of these proinflammatory cytokines was initially the same for both strains in the liver and heart (Fig. 4). By day 3 postinfection, BALB/c mice were producing significantly more IL-6 in all their organs and more TNF-α in their lungs and livers than C57BL/6 mice (Fig. 4). However, though both mouse strains induced high amounts of TNF-α mRNA in their livers and hearts on the day before succumbing to infection, BALB/c mice also induced significantly higher amounts of IL-6 in their livers and hearts (Fig. 4e–i). Moreover, BALB/c mice also induced more IL-1 mRNA in their livers and hearts, but this difference was not statistically significant (Fig. 4b and c). Together, these results suggest that increased mortality of BALB/c mice is associated with greater induction of the proinflammatory cytokines, IL-6 and IL-1, in their organs compared with C57BL/6 mice.

Macrophages play a critical role in the host defense against *F. novicida*, but they also produce proinflammatory cytokines such as RANKL, which promote calcification. We therefore determined whether lung macrophages contribute to the development of DCC during pulmonary tularemia by administering aerosolized clodronate-containing liposomes (CLL) 2 days before infection as described previously (Leemans *et al.*, 2001). Depletion of lung macrophages prior to *F. novicida* challenge significantly impaired DCC in BALB/c compared with controls treated with PBS-containing liposomes (Fig. 5b and c). These findings indicate that the lung macrophages are involved in pathogenesis of DCC in BALB/c mice. Interestingly, macrophage-depleted BALB/c mice did not show increased mortality to respiratory *F. novicida* challenge, suggesting that macrophages may not be the only cells involved in innate host defense against *F. novicida* (Fig. 5a).

In summary, we show that C57BL/6 mice are relatively more resistant to pulmonary *F. novicida* infection than BALB/c mice but they eventually succumb to infection. Furthermore, *F. novicida* causes pneumonia and liver damage in both mouse strains but it disseminates to the heart and induces rapid pericarditis and DCC in BALB/c mice, which appears to be related to deficient osteopontin production in these mice. Finally, the data show that lung macrophages are involved in inducing DCC in BALB/c mice. To the best of our knowledge this is the first report to show that acute respiratory infection with *F. novicida* induces rapid cardiac damage and calcification.

Acknowledgments

We thank Dr John Gunn for generously providing the *F. novicida* strains and Dr Richard Mortensen and Heidi Snider for critical review of the manuscript. This work was sponsored by the NIH/NIAID Regional Center of Excellence for Bio-defense and Emerging Infectious Diseases Research (RCE) Program. The author (J.S.G.) wishes to acknowledge membership within and support from the Region V ‘Great Lakes’ RCE (NIH award 1-U54-AI-057153).

Statement This research was supported by National Institutes of Health/University of Minnesota PRCE Research Grant and Tzagournis Medical Research Fund. The Authors declare no conflict of interest.

References

Aherrahrou Z, Axtner SB, Kaczmarek PM, Doehring LC, Weichenhan D, Katus HA, Ivandic BT. A locus on chromosome 7 determines dramatic up-regulation of osteopontin in dystrophic cardiac calcification in mice. Am J Pathol. 2004; 164:1379–1387. [PubMed: 15039225]

Beck SE, Laube BL, Barberena CI, Fischer AC, Adams RJ, Chestnut K, Flotte TR, Guggino WB. Deposition and expression of aerosolized rAAV vectors in the lungs of Rhesus macaques. Mole Ther. 2002; 6:546–554.

Collin-Osdoby P. Regulation of vascular calcification by osteoclast regulatory factors RANKL and osteoprotegerin. Circ Res. 2004; 95:1046–1057. [PubMed: 15564564]

Dennis DT, Inglesby DA, Henderson JG, et al. Tularemia as a biological weapon-medical and public health management. JAMA. 2001; 285:2763–2773. [PubMed: 11386933]

Giachelli CM, Speer MY, Li X, Rajachar RM, Yang H. Regulation of vascular calcification: roles of phosphate and osteopontin. Circ Res. 2005; 96:717–722. [PubMed: 15831823]

Hall WC, Kovatch RM, Schricker RL. Tularaemic pneumonia: pathogenesis of the aerosol-induced disease in monkeys. J Pathol. 1973; 110:193–201. [PubMed: 4200656]

Ilback NG, Friman G, Beisel WR, Johnson AJ, Berendt RF. Modifying effects of exercise on clinical course and biochemical response of the myocardium in Influenza and Tularemia in mice. Infect Immun. 1984; 45:498–504. [PubMed: 6746102]

Ivandic BT, Qiao J-H, Machleder D, Liao F, Drake TA, Lusis AJ. A locus on chromosome 7 determines myocardial cell necrosis and calcification (dystrophic cardiac calcinosis) in mice. Proc Nat Acad Sci USA. 1996; 93:5483–5488. [PubMed: 8643601]

Ivandic BT, Utz HF, Kaczmarek PM, Aherrahrou Z, Axtner SB, Klepsch C, Lusis AJ, Katus HA. New *Dyscalc* loci for myocardial cell necrosis and calcification (dystrophic cardiac calcinosis) in mice. Physiol Genomics. 2001; 6:137–144. [PubMed: 11526197]

Lamps LW, Havens JM, Sjostedt A, Page DL, Scott MA. Histologic and molecular diagnosis of tularemia: a potential bioterrorism agent endemic to North America. Modern Pathol. 2004; 17:489–495.

Leemans JC, Juffermans NP, Florquin S, van Rooijen N, Vervoordeldonk MJ, Verbon A, van Deventer SJ, van der Poll T. Depletion of alveolar macrophages exerts protective effects in pulmonary tuberculosis in mice. J Immunol. 2001; 166:4604–4611. [PubMed: 11254718]

O'Regan S, Berman JS. Osteopontin: a key cytokine in cell-mediated and granulomatous inflammation. Int J Exp Path. 2000; 81:373–390. [PubMed: 11298186]

Shen H, Chen W, Conlan JW. Susceptibility of various mouse strains to systemically- or aerosol-initiated tularemia by virulent type A *Francisella tularensis* before and after immunization with the attenuated live vaccine strain of the pathogen. Vaccine. 2003; 22:2116–2121. [PubMed: 15149767]

Zhu Y, Denhardt DT, Cao H, Sutphin PD, Koong AC, Giaccia AJ, Le Q-T. Hypoxia upregulates osteopontin expression in NIH-3T3 cells via a Ras-activated enhancer. Oncogene. 2005; 24:6555–6563. [PubMed: 16007184]

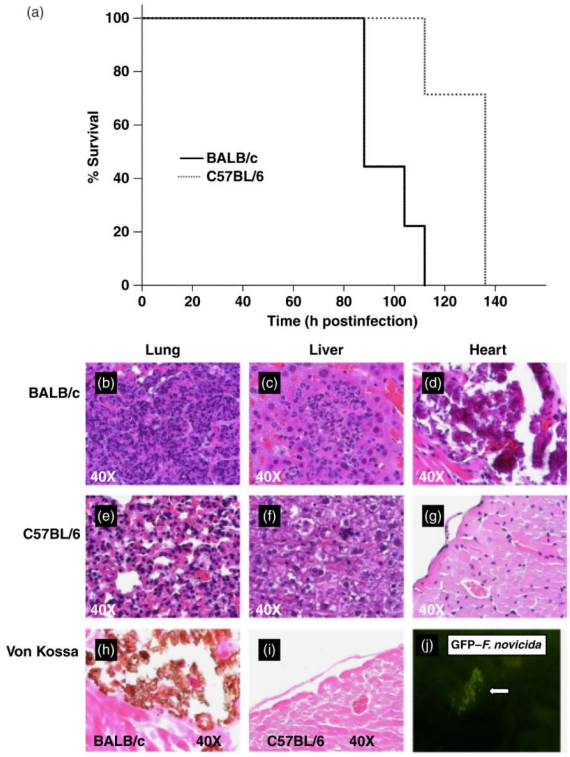

Fig. 1.

Survival curves (a) and histopathology of lungs, heart and liver (b–i) from BALB/c and C57BL/6 mice following aerosolized *Francisella novicida* infection. (a) The survival of BALB/c (solid line) and C57BL/6 (dotted line) mice infected with 10^3 CFU of aerosolized *F. novicida* were compared. Groups of 10 BALB/c and 10 C57BL/6 mice were monitored in this experiment. Statistical significance was determined using a Log-Rank test, ($P < 0.001$). Histological analysis of *F. novicida*-infected lung, liver and heart tissue from BALB/c (b–d and h) and C57BL/6 (e–g and i) mice are shown. Both hematoxylin and eosin staining of all three organs and von Kossa staining for heart calcium deposition (brown) are shown for BALB/c and C57BL/6 mice at day 4 postinfection. (j) Detection of GFP-*F. novicida* in the infected pericardium of BALB/c mice by immunofluorescence microscopy. Similar results were observed in three independent experiments.

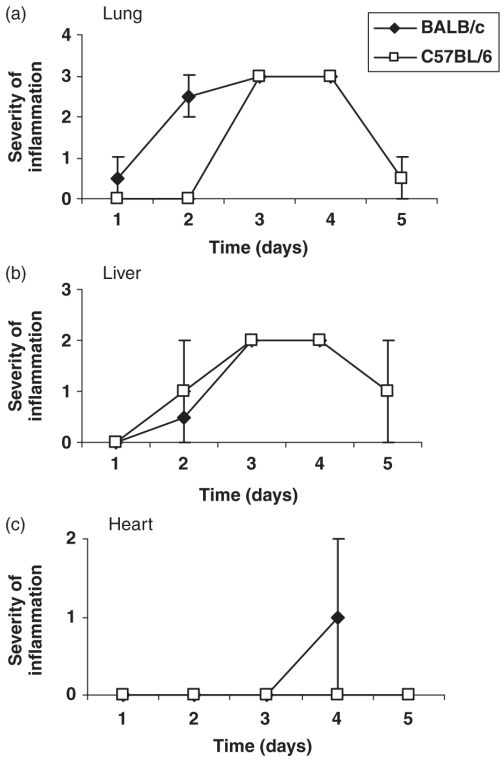

Fig. 2.

Comparison of the severity of inflammation in lungs, livers and hearts from *Francisella novicida*-infected C57BL/6 and BALB/c mice. The severity of pathology in the lungs, liver and heart (a–c) of both strains of mice were compared temporally. H&E stained slides of the organs were blinded and scored by a pathologist and then plotted over time. The data are from two independent experiments.

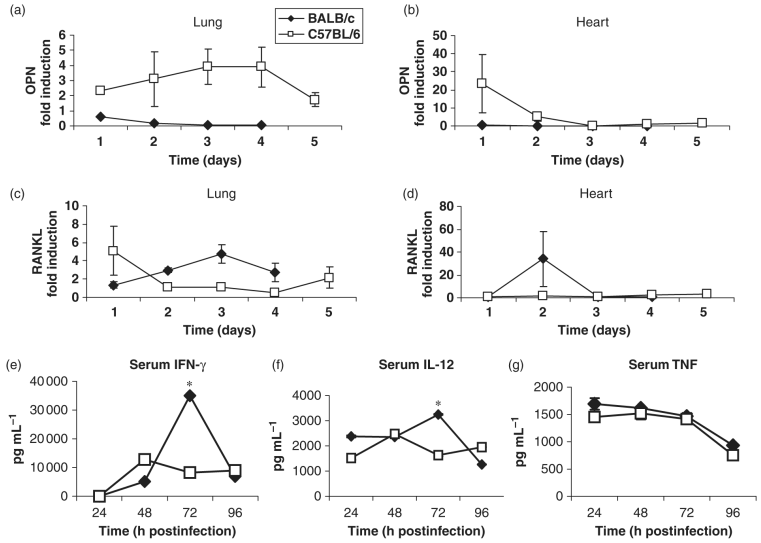

Fig. 3.

Quantification of osteopontin and RANKL mRNA levels in the infected hearts and lungs (a–d) and serum cytokine levels (e–g) in BALB/c and C57BL/6 mice. (a) Real-time RT-PCR analysis was used to measure the induction of osteopontin and RANKL mRNA in the lungs (a and c) and hearts (b and d) of BALB/c (diamonds) and C57BL/6 (squares) mice following aerosol infection with 10^3 CFU *Francisella novicida*. Results were normalized to the housekeeping gene, β-actin, and presented as fold induction over uninfected BALB/c or C57BL/6 mice. The results are the mean (± SEM) of triplicate samples from five or six mice per group for each time interval collected for two independent experiments. The kinetics of serum cytokine changes in BALB/c (diamonds) and C57BL/6 (squares) mice following *F. novicida* aerosol infection were determined using ELISA. Mice were bled on days 1, 2, 3 and 4 after infection and levels of IFN-γ (e), IL-12p70 (f) and TNF-α (e) were measured in the serum by ELISA. Data show the mean (± SEM) of triplicate samples from five or six mice per group from two independent experiments.

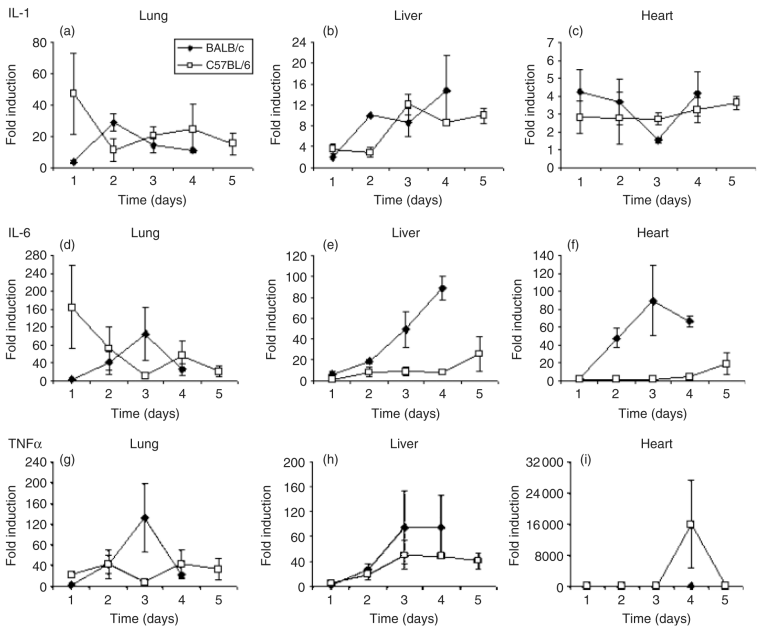

Fig. 4.

Quantification of IL-1, IL-6 and TNF-α mRNA levels in the infected lungs, livers and hearts of BALB/c and C57BL/6 mice. Real-time RT-PCR analysis was used to measure the induction of IL-1, IL-6 and TNF-α mRNA in the lungs (a, d, g), livers (b, e, h) and hearts (c, f, I) of BALB/c (diamonds) and C57BL/6 (squares) mice following aerosol infection with 10^3 CFU *Francisella novicida*. Results were normalized to the housekeeping gene, β-actin, and presented as fold induction over uninfected BALB/c or C57BL/6 mice. The results are the mean (± SEM) of triplicate samples from five or six mice per group for each time interval collected for two independent experiments.

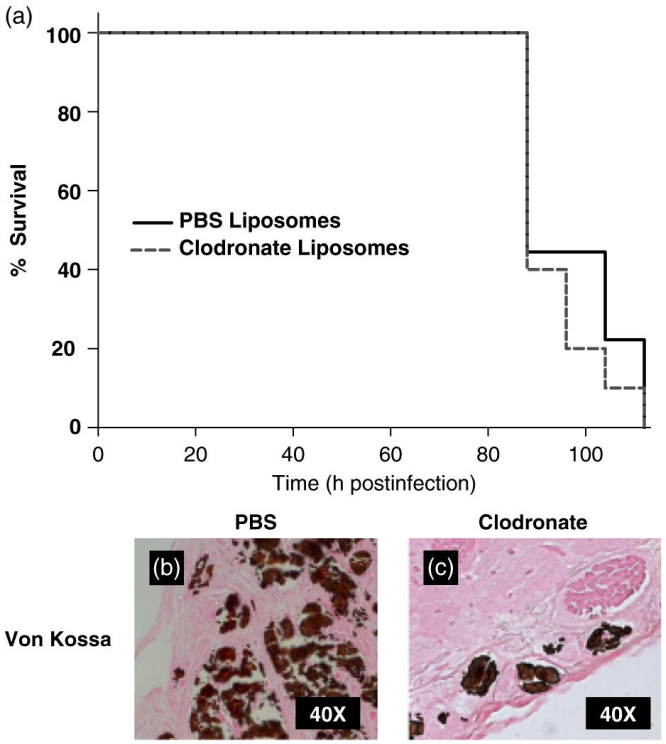

Fig. 5.

Survival curves (a) and histopathological analysis of calcification in the heart after lung macrophage depletion (b, c). BALB/c mice were treated with either clodronate-containing liposomes or PBS-containing liposomes two days prior to infection with 10^3 aerosolized *Francisella novicida* in order to deplete lung macrophages. (a) The survival of groups of ten clodronate-treated (dotted line) and PBS-treated (solid line) mice were compared in this experiment. Using a Log-Rank test, it was determined that there was not a statistically significant difference in survival ($P < 0.398$). Von Kossa staining of the heart tissue from PBS-treated (b) and clodronate-treated (c) mice are shown at the time of death. Similar survival rates and calcium deposition were noted in two independent experiments.